Modeling electron beam irradiation of methane

Weiyao Gu (wgu100@syr.edu) and Theodore S. Dibble* (tsdibble@esf.edu)

State University of New York College of Environmental Science and Forestry

Highlights

- A chemical kinetic model for the electron beam irradiation of methane was built
- The G-value of stable products (H_2, C_2H_4, C_3H_6, C_3H_4, C_2H_2, C_3H_8, C_2H_6, and C_4H_{10}) was reported
- Reactions produce and destroy H_2, C_3H_6, and C_2H_6 were identified
- A mechanism reduction has been performed based on normalized sensitivity coefficients (NSC).

Abstract

We built a chemical kinetic model for the electron beam irradiation of methane and report simulation results with dose rates ranging from 2 to 200 kGy sec^{-1} at 298 K and 1 atm pressure. The model contains 92 species and 778 gas-phase reactions. We report the time evolution of concentrations of stable products (including H_2, C_2H_6, C_3H_8, C_2H_4, C_3H_6, C_4H_{10}, C_2H_2, and C_3H_4) as well as some radicals and ions. We discuss how yields of products depend on dose rate and how they change during the course of irradiation. To understand the processes controlling product formation, we quantify the extent to which various reactions produce and destroy major products and the key radicals and ions. Normalized sensitivity coefficients (NSC) are computed for the production of stable products to gain further insight into factors controlling product yields. We were able to reduce the mechanism to 63 species and 331 reactions while incurring less than 5% error in the final concentrations of stable products.

Keywords

Kinetic model, electron beam, irradiation, methane, mechanism reduction

1. Introduction

The irradiation of methane has a large potential for industrial applications[1]. Methane is the dominant component of natural gas, whose price has dropped in recent years due to increased production from hydrofracking[2]. Radiation-induced free radical chain reactions can convert methane to higher hydrocarbons[3]. Methane conversion to higher hydrocarbons could provide new options for chemical processes and decrease the cost of transportation fuels[4]. One of the most promising methods of irradiation of methane is electron beam irradiation. The electron beam is a mature technology with many industrial applications[5] and can be designed for any of a wide range of energies (200 keV to 10 MeV)[6]. Electron beam exhibits high efficiency (approaching 80%) for conversion of electrical power to electron energy[7]. Unlike the discharge-based plasma technologies,

such as dielectric barrier discharges (DBD), radio frequency, and microwave[8–10], which are mostly limited to small-scale applications, electron beam technology is already used for industrial-scale processing[11, 12].

Experimental research on methane radiolysis by electron beams has been carried out for over half a century. Potential valuable products from the radiolysis include H_2 and C_2 and C_3 hydrocarbons[13–15]. Experiments provide gas chromatographic measurements of yields for H_2 and other hydrocarbons[14–17]. However, our understanding of methane radiolysis remains very incomplete. Experiments usually analyze no more than a handful of stable products or a few reactive species, and their proposed mechanisms of reactions of primary products of radiolysis are conjectures[13–15]. Plausible conjectures include the involvement of ions or radicals in the reactions forming stable products[16, 17].

Kinetic modeling is a powerful tool to study a complex reaction system[18–22]. The most commonly used CH_4 plasma, dielectric barrier discharges (DBDs), has been modeled under various conditions[18, 19]. Kinetic modeling provides insight of radical–involved reaction pathways in combustion chemistry[21, 22]. Previous modeling works have been developed on the processing of methane by sources other than the electron beam. In addition to DBDs, Heijkers et al. built a kinetic model for CH_4 conversion using microwave and gliding arc plasmas to understand reaction mechanisms, predicting that thermal conversion is more important than vibrational–translational nonequilibrium in CH_4 plasmas[23]. However, there has not been a comprehensive modeling effort of electron beam of methane, though experimental data have being available for a long time [14–17].

We developed a kinetic model for simulating methane radiolysis and carried out simulations for a wide range of dose rates. In a real-world scenario, there is a spatial variation of energy deposition inside the electron beam reactor. The energy is higher near where the electrons first interact with the gas than at longer distances and is also higher along the direct path of the beam than off to the sides. The range of dose rates simulated here can be used to shed light on the spatial variation of product yields, but does not account for the influence of fluid dynamics on concentrations or how the reactor walls would affect dose rates.

Our major goal of this work is to identify the most important reactions forming products in electron-beam irradiation of pure CH_4. The mechanism developed here could help guide the selection of experimental conditions for optimizing product yields. Additionally, our model could serve as a basis for radiolysis of mixtures of CH_4 with other gases, such as CO_2 to transform this greenhouse gas to commodity chemicals (methanol, acetic acid etc.), accompanying with production of syngas and H_2 for fuel cells[1, 24]. Understanding methane radiolysis is a first step towards this goal.

We will first report on the time history of concentrations of products, including radicals and ions. Yields of stable products are compared to experimental data. Our initial discussion focuses on the condition of a dose rate of 50 kilogray per second (kGy s^{-1}, 1 Gy = 1 kJ of absorbed energy per kg of material), but we later discuss how results vary with dose rate. We then report the reactions controlling formation and destruction of stable products, and compare results to previously conjectured mechanisms. Finally, we report on efforts to condense the mechanism.

2. Methods

Model description

The simulations treat a wide range of dose rates: from 2 to 200 kGy sec^{-1}. We use a fixed temperature at 298 K. The total initial pressure of CH_4 is set to 1 atm. The gas residence time in most of the simulations will be 0.5 s. The software we used for our kinetic modeling was Kintecus (version 6.80 http://www.kintecus.com/index.htm). Kintecus is a compiler for modeling multiple types of chemical reactions[25]. The program uses a DASPK integrator to carry out numerical integration. We used a numerical accuracy of 1.0×10^{-5}.

The full model contains 782 reactions and 94 species. The complete set of reactions can be found in **Table S1**. Yields of products from methane fragmentation to first-generation products by the electron beam were taken from the work of Okazaki et al.[26]:

$$7.24CH_4 + 100\ eV \rightarrow 3.94H + 2.34H_2 + 2.05CH_3 + 1.63CH_4^+ + 1.43CH_3^+ + 1.27CH_2 + 0.48CH + 0.32CH_2^+ + 0.16C + 0.11H^+ + 3.51e^- \quad (1)$$

Their results for NH_3 and H_2O, computed in the same paper, were fairly close to those compiled by Willis and Boyd[20], so we believe they are fairly reliable.

The "e^-" in the products Equation 1 represents the hot electron with an energy of a few eV. Hot electrons are thermalized by collisions with CH_4 molecules[26]. We treat the quenching of the hot electron to the thermal electron (et^-) as a pseudo-first-order reaction[27]. Due to the complexity and lack of data, we do not include the physics of vibrational excitation of methane by the electron beam or the subsequent evolution of the vibrational population[10, 28]. Even at the highest dose rate (200 kGy sec^{-1}), the destruction of CH_4 is less than 0.01% of total CH_4; as a result, we neglect its loss to radiolysis in these simulations.

For the simulations, we generate a set of reactions to represent the primary radiolysis events. For instance, one of the ionization reactions during the primary radiolysis can be represented as:

$$\text{Source} \rightarrow CH_3^+ + H + e^- \quad (2)$$

where "Source" corresponds to the rate of energy deposition calculated from the dose rate in units of 100 eV cm^{-3} sec^{-1}, and the rate constant is simply the number of molecules changed for each 100 eV energy absorbed for primary products of radiolysis in Equation (1).

Set of assumptions

The reaction types in the model are electron-neutral reactions, ion-neutral reactions, ion-ion reactions, electron-cation reactions, and neutral-neutral reactions. We searched for rate constants for neutral-neutral reactions in the JPL Data Evaluation and NIST Chemical Kinetics Database. Rate constants for most of the reactions involving ions or electrons were obtained from the compilation of experimental data by Anicich (~ 42 reactions)[29] or the Kinetic Database for Astrochemistry

(KIDA, ~ 440 reactions). To minimize bias in the selection of rate constants, we applied two rules: 1) The rate constants from experimental works are selected over theoretical ones. 2) The most recent rate constants are selected over older ones. For thermodynamically favorable second-order ion reactions with no available product yield data, we assign a product set with a negative reaction enthalpy < 100 kJ mol^{-1}. We do not account for species larger larger than C4, except for benzene, its cation, and protonated benzene. We do not keep track of isomers for C3/C4 species, and their concentrations are displayed as the total concentration. For example, the mechanism only includes on C_3H_4 species, which lumps together propadiene, methylacetylene and cyclopropane. Where rate constants have not been reported, we determine the value by reaction type: electron-neutral reactions (5×10^{-11} cm^3 $molecule^{-1}$ s^{-1}), anion-neutral reactions (1×10^{-10} cm^3 $molecule^{-1}$ s^{-1}), cation-neutral reactions (1×10^{-9} cm^3 $molecule^{-1}$ s^{-1}), and anion-cation reactions (1×10^{-8} cm^3 $molecule^{-1}$ s^{-1}), respectively. These values are estimated based on other known rate constants within the same reaction category. The lack of kinetic and product yield data represents a major limitation of the current model.

Production/destruction analysis

To quantify the influence of various reactions on the production and destruction of key product species, we add "tracers" as products of selected reactions in the model. For example, we add the tracer R2 to the reaction (2):

$$\text{Source} \rightarrow CH_3^+ + H + e^- + R2 \qquad (2)^*$$

R2 and other tracers are treated as a chemical species in the simulation. The concentration of the tracer at any time in the simulation corresponds to the time-integrated rate of reaction. Details of this method were described in Schmitt et al. (2009)[30].

Model reduction

We perform a mechanism reduction using the Atropos software (http://www.kintecus.com/atropos.htm). A detailed explanation of the software can be found in Ianni and Didion et al.[31, 32], but we present a short explanation here. The first step is to compute normalized sensitivity coefficients (NSCs). NSCs show how the rate constants in the model influence a product's concentration at a given time. The NSC at any one time during the simulation is defined as the value of [25]:

$$NSC = \left(\frac{\frac{\partial[Species]}{[Species]}}{\frac{\partial k}{k}}\right)_{k'} = \left(\frac{\partial ln[Species]}{\partial ln\, k}\right)_{k'} \qquad (3)$$

where [Species] is the concentration of species of interest, k is the rate constant of a specific reaction, and k' are all other rate constants. The NSC forms an array S at each selected time point. Eigenvalue-eigenvector decomposition is obtained by the diagonalization of the matrix S^TS. Atropos eliminates unimportant reactions that are elements of eigenvectors[25] corresponding to eigenvalues less than 10^{-4}.

3. Results and discussion

Performance and validation of the model

As mentioned in the Methods section, the initial CH_4 concentration is set to be 1 atm. through all our simulation, and only ~0.01% of CH_4 has been destroyed in the end of our simulation. The time evolution of the concentrations of the eight most abundant stable products at a dose rate of 50 kGy sec^{-1} is shown in **Figure 1**. These eight products account for over 99% of total products at the end of the simulation. H_2 constitutes 62.0% of the products, followed by C_2H_6 (ethane, 22.6%) and C_3H_8 (propane, 6.5%). Other hydrocarbon species produced in decreasing order of abundance are C_2H_4, C_3H_6, C_4H_{10}, C_2H_2, and C_3H_4. The concentrations of all the most abundant products increase steadily with time.

Figure 2 shows the time evolution of the concentrations of the five most abundant neutral radicals (CH_3, H, C_2H_5, C_3H_3, and CH_2) at 50 kGy sec^{-1}. These five radicals account for over 90% of total radicals produced. Note that [H] and [CH_3] in **Figure 2** are shown at $1/10^{th}$ their actual value, so their concentrations are much greater than those of other radicals at all simulation times. The concentration of atomic hydrogen increases rapidly in the first 0.016 seconds, then decays by ~93% over the remainder of the 0.5-sec simulation. By contrast, the concentration of methyl radical reaches an approximate steady-state by 0.016-second. Concentrations of C_2H_5, C_3H_3, and CH_2 do not exhibit a quick rise, rather, their concentrations rise steadily over the course of the simulation.

Let us consider the reasons for this behavior. Atomic hydrogen and CH_3 radicals form directly from the radiolysis of CH_4, which produces them at a fast and constant rate. Because these radicals react only very slowly with CH_4, at short times their loss is dominated by reaction with each other. Thus, the increase in [H] prevents the accumulation of CH_3, as the reaction with H is a sink for CH_3. But why does [H] increase rapidly and then decrease? Looking back at equation (1), we see that the rate of production of H is ~two times higher than the rate of CH_3. However, atomic hydrogen reacts more rapidly than CH_3 with second-generation radicals (those formed from first-generation reactive species rather than from radiolysis). Because of the accumulation of second-generation radicals and ions after 0.016 seconds, the concentration of H decreases sharply by reaction with these species.

Figure 3 depicts the time evolution of concentrations of the most abundant ions ($C_2H_7^+$, $C_3H_7^+$, et^-, $C_3H_5^+$, $C_2H_5^+$, and H^-) at 50 kGy sec^{-1}. Thermalized electron dominates the concentration of negatively charged species and that its concentration changes little after its initial spike. This is because CH_4 and H_2 possess negative electron affinities, so thermalized electrons can only react with trace species. Turning our attention to the cations, we see that $C_2H_7^+$ has the highest concentration (over 8.0×10^{10} molecules cm^{-3}) among cations, followed by $C_3H_7^+$, $C_3H_5^+$, and $C_2H_5^+$. Concentrations of the first-generation cations H^+, CH_4^+, CH_3^+, and CH_2^+ (**Figure S1**) reach a steady state in less than one microsecond and constitute less than 10^{-6} of the total ion concentration. Unlike the first-generation radicals, first-generation ions react rapidly with CH_4, thereby keeping the first-generation cations at low concentrations.

To evaluate the model's performance, we compare its results (as G-values) to those obtained in experimental work under a range of experimental conditions (**Table 1**)[14–17]. **Figure 4** shows a comparison of G-values between the model's result and electron beam experiments. G-values of products variy among the four experiments. This variation could be caused by pressure, gas residence time, energy input, etc. The relative abundance of stable products from the model's

prediction agrees with experimental results. In general, the model predicts higher G-values than the corresponding experiment, especially for C_3H_8. Since information about the radiolysis time is not always clearly stated in these papers[15–17], some of this discrepancy might be attributed to our choice of a simulation time. As shown in **Figure S2**, G for the production of C_3H_8 decreases from 0.89 to 0.57 in changing from a 0.5-second to a 6-second simulation. Similarly, G for the production of stable products decreases as increasing in dose rate, with the exception of C_4H_{10} (**Figure S3**).

Production/destruction mechanism of H_2 and C_2H_6

Above, we discussed the processes controlling the product concentrations and G-values of classes of products. In the following section, by the use of tracers, we quantify the role of individual reactions in the production and destruction of particular products. In the text we discuss results for the two most abundant products (H_2 and C_2H_6,), but results for other stable products are presented in the Supporting Information. The source reaction (radiolysis of CH_4) directly produces 27% of the H_2 for 0.5-second simulations at 50 kGy/sec. Although 225 chemical reactions contribute to its production, 95% of H_2 production comes from only 12 reactions, of which the top three reactions account for 48%, (**Figure 5**). These production reactions are sorted by rank in **Table 2**.

Anicich evaluated rate constants for reactions (4) and (5)[29]. Although these reactions appear analogous (both involved alkyl cations reacting with CH_4), reaction (4) has a much smaller rate constant than (5). The reason might be that reaction (5) is a highly exothermic reaction ($\Delta_rH^\ominus$ = -117.8 kJ mol^{-1}, 298 K) and reaction (4) is much less exothermic ($\Delta_rH^\ominus$ = -22.8 kJ mol^{-1}, 298 K)[29, 33].

Curiously, reaction (4), the reaction in Table 2 with the smallest rate constant, contributes more H_2 (19%) than reaction (5) (18%) for 0.5-second simulations at 50 kGy sec^{-1}. As mentioned earlier, the concentration of $C_2H_5^+$ (reactant in reaction (4)) is much higher than that of CH_3^+ (reactant in reaction 5). The higher abundance of $C_2H_5^+$ more than offsets the effect of smaller rate constants in reaction (4). Reactions (4) and (5) had previously been suggested as important sources of H_2[14, 15]. Sieck and Johnsen proposed two H_2-producing mechanisms:

$$H + CH_4 \rightarrow H_2 + CH_3 \quad (k = 9.0 \times 10^{-14}\ cm^3\ molecule^{-1}\ s^{-1}) \tag{7}$$

$$H + H + M \rightarrow H_2 + M \quad (k = 1.7 \times 10^{-17}\ cm^3\ molecule^{-1}\ s^{-1}) \tag{8}$$

which are included in our model. However, our simulations indicated that reactions (7) and (8) contribute less than 0.3% of total H_2 production. The relative lack of importance of these reactions is due to high barrier of reaction (7) and the dependence of the rate of reaction (8) on the square of the (low) concentration of H.

Our simulation predicts the destruction of H_2 only removes 0.1% of the total H_2 formed. In contrast to the enormous number of reactions producing H_2, only 32 reactions destroy H_2, as shown in **Figure S4**. Reactions between H_2 and first-generation radicals are the most important destruction mechanisms of H_2.

Table 3 shows the relative importance of C_2H_6 production reactions at 50 kGy sec^{-1}. Five reactions (out of a total of 16) contribute ~99% to total C_2H_6 production. Reactions (9), (10), and

(12) account for 65%,16%, and 12%, respectively, of total C_2H_6 production in the 0.5-second simulation. The importance of reactions (9) and (10) decreases in the 6-second simulation (to 52% and 13%), while the contribution of reaction (11) rises from 5% to 20%. Our results confirm the conjectures of previous work about the importance of reactions (9) and (10)[13, 15, 34, 35] and reaction (12) (see **Table 3**)[14]. As reactions (11) and (13) show, the production of ethane is also affected by reactions between cations and stable products. The increase in the relative importance of reaction (11) with increasing radiolysis time reflects the accumulation of propane with time.

A previous paper claimed that reaction (14), involving the singlet excited state of CH_2:

$$^1CH_2 + CH_4 + M \rightarrow C_2H_6^* + M \rightarrow C_2H_6 \quad (14)$$

is important for ethane production[13, 14]. However, the influence of $^1CH_2$ is uncertain. There are multiple potential products of the reaction $^1CH_2 + CH_4$, including quenching to $^3CH_2 + CH_4$ and formation of $CH_3 + CH_3$; the branching ratios between these products are not well-known[36]. Also, the only likely source of $^1CH_2$ is radiolysis, and it is unclear to what extent radiolysis form $^1CH_2$ versus ground state CH_2 ($^3CH_2$). Consequently, we exclude $^1CH_2$ and reaction (14) from the model to avoid introducing bias while acknowledging the resulting uncertainty. Our analysis indicates that the reaction $CH_4 + C_2H_5 \rightarrow CH_3 + C_2H_6$, suggested by Arai et al. and Cahill et al.[13, 16], contributes negligibly to ethane formation, on account of its very low rate constant ($\sim 10^{-24}$ molecules^{-1} cm^3) at room temperature. The rate constant does increase at higher temperatures; however, it does not increase enough to make this reaction significant even at the 120 °C conditions of Arai et al. (120 °C).

Although destruction of H_2 scarcely affects its concentration (**Figure S4**), our simulation predicts the destruction of ethane significantly reduces its final concentration (by 29%, see **Figure S5**). Our model suggests the destruction of ethane comes from the reactions of ethane with CH_5^+ cation, which drew little attention in previous papers:

$$C_2H_6 + CH_5^+ \rightarrow H_2 + CH_4 + C_2H_5^+ \quad (15)$$

$$C_2H_6 + CH_5^+ \rightarrow CH_4 + C_2H_7^+ \quad (16)$$

Thus, a good estimate of $[C_2H_6]$ can be achieved by considering just four production reactions and one destruction reaction:

$$d([C_2H_6])/dt = k_9[CH_3]^2 + k_{10}[H][C_2H_5] + k_{11}[C_2H_5^+][C_3H_8] - (k_{15} + k_{16})[C_2H_6][CH_5^+] \quad (17)$$

Due to the lack of other comprehensive electron beam modeling of CH_4 radiolysis, we compare our important reaction pathways alternatively to a most recent DBD CH_4 modeling work by Heijkers et al.[23] in **Table 4.** According to Heijkers et al., electron-neutral reactions account for the loss of H_2 and C_2H_6[23]. However, because of the low extent of CH_4 loss in our simulation, electron-neutral reactions contribute <0.1% to overall C_2H_6 destruction process in the electron beam model (assuming the primary radiolysis rate of C_2H_6 is as same as CH_4) and the ethane destruction is mainly caused by CH_5^+ ion in our model (Reactions 15 and 16).

Model reduction

We performed a mechanism reduction using the program Atropos[32]. **Table 5** shows the percent difference in concentration of stable products between the original model of 778 reactions and reduced mechanisms containing 186 to 359 reactions. The model size decreases as we apply increasingly loose accuracy thresholds in Atropos. These simulations modeled a dose rate of 50 kGy sec^{-1} for six seconds. None of these reduced mechanisms introduced significant deviation for H_2 (<2%). For other stable species, there is very little difference between the full mechanism and a mechanism of as few as 331 reactions (63 species instead of 92) at any time during the simulation. Reducing the model to 247 and 300 reactions causes significant (-7% to -36%) deviations for C_2H_4 and C_2H_2. Further reducing the model to 186 reactions increases the deviation to more than -95% for these two species, corresponding to underestimates of 36 and 67 for C_2H_4 and C_2H_2, respectively. To this point, we are confident to say one can condense the model to 63 species and 331 reactions while incurring no more than 5% error in the final concentrations of stable products.

By the standards of chemical mechanisms routinely used in fluid dynamics simulations of combustion, 331 reactions is rather large[37–39]. However, radiolysis has modest spatial and temporal gradients in chemical composition and energy deposition as compared to combustion, so we suspect that this reduced model can be combined with 3-dimensional fluid dynamics in simulations.

4. Conclusion

We built a model of electron beam radiolysis chemistry of pure methane. We performed kinetic modeling of radiolysis across a wide range of dose rates (2-200 kGy sec^{-1}) at 298 K and 1 atmosphere. The most abundant stable product is H_2, with C_2H_6 being the next most abundant at 50 kGy sec^{-1}. The relative abundance of stable products from the model's prediction agrees with experimental results. We investigated the production of other important stable products, as well as radicals and ions. Except for C_4H_{10}, The G-value of the stable products decreases modestly when varying the radiolysis time from 0.5 to 6 seconds and from 2 to 200 kGy sec^{-1} of the simulation. We suggest that the production of H_2 is largely controlled by reactions between cations and CH_4, instead of previous conjectured reactions H + CH_4 or H + H + M. The relative lack of importance of these reactions is due to high barrier of H + CH_4 and the dependence of the rate of H + H + M on the square of the (low) concentration of H. We confirm that CH_3 + CH_3 and H + C_2H_5 as important C_2H_6-producing mechanism. Our analysis indicates that the previous conjectured reaction CH_4 + $C_2H_5 \rightarrow CH_3 + C_2H_6$, contributes negligibly to ethane formation, on account of its very low rate constant ($\sim 10^{-24}$ cm^3 $molecules^{-1}s^1$) at room temperature. Our model suggests the destruction of ethane comes from the reactions of ethane with CH_5^+ cation, which drew little attention in previous papers. We find that the contributions of reactions directly producing or destroying H_2 and C_2H_6 are highly concentrated, with over 90% of production or destruction of these products being due to only a few reactions.

A sensitivity analysis (see Supporting Information) was used to generate reduced models, which should simplify efforts to improve the chemical mechanism. We successfully reduced the size of the model from 92 species and 778 reactions to 63 species and 331 reactions while incurring no more than 5% error in the final concentrations of stable products. This reduced model could help overcome the challenges imposed by small integration time steps when modeling pulsed radiolysis. The reduced mechanism could also be coupled with fluid dynamics in future studies of continuous methane radiolysis.

Limitations on the reliability of this work include: 1) the lack of literature data on rate constants and products of many relevant reactions 2) ignorance of the influence of fluid dynamics on concentrations or how the reactor walls would affect dose rates. Nevertheless, we hope that this serves as a steppingstone towards more reliable modeling of methane radiolysis.

Acknowledgment

This work was supported by DOE Contract No. DE-FE0029787 under a sub-contract from the Gas Technology Institute.

Data Availability Statement

Data available in article supplementary material.

REFERENCES

1. Jun, J., Kim, J. C., Shin, J. H., Lee, K. W., & Baek, Y. S. (2004). Effect of electron beam irradiation on CO2 reforming of methane over Ni/Al2O3 catalysts. *Radiation Physics and Chemistry*, 71(6), 1095-1101. https://doi.org/10.1016/j.radphyschem.2003.07.006

2. Belyadi, H., Fathi, E., & Belyadi, F. (2019). Hydraulic fracturing in unconventional reservoirs: Theories, operations, and economic analysis (Second ed.). *Gulf Professional Publishing, an imprint of Elsevier*

3. Wang, K., Damarla, H. R., Berman, I. C., & Staack, D. (2020). High dose rate electron beam irradiation of heavy alkanes in a multi-phase flow system. *Fuel (Guildford)*, 274, 117695. https://doi.org/10.1016/j.fuel.2020.117695

4. Derk, A. R., Funke, H. H., & Falconer, J. L. (2008). Methane conversion to higher hydrocarbons by UV irradiation. *Industrial & engineering chemistry research*, *47*(17), 6568-6572.

5. Vayre, B., Vignat, F., & Villeneuve, F. (2012). Metallic additive manufacturing: state-of-the-art review and prospects. *Mechanics & Industry*, 13(2), 89-96. https://doi.org/10.1051/meca/2012003

6. Spinks, J. W. T. (1990). Water and inorganic aqueous systems. *Introduction to radiation chemistry*. https://doi.org/10.1126/science.146.3645.760

7. Negi, S., Nambolan, A. A., Kapil, S., Joshi, P. S., R, M., Karunakaran, K. P., & Bhargava, P. (2020;2019;). Review on electron beam based additive manufacturing. *Rapid Prototyping Journal*, 26(3), 485-498. https://doi.org/10.1108/RPJ-07-2019-0182

8. Ramakers, M., Michielsen, I., Aerts, R., Meynen, V., & Bogaerts, A. (2015). Effect of argon or helium on the CO2 conversion in a dielectric barrier discharge. *Plasma Processes and Polymers*, *12*(8), 755-763. https://doi.org/10.1002/ppap.201400213

9. Kozák, T., & Bogaerts, A. (2014). Splitting of CO2 by vibrational excitation in non-equilibrium plasmas: a reaction kinetics model. *Plasma Sources Science and Technology*, *23*(4), 045004. https://doi.org/10.1088/0963-0252/23/4/045004

10. Lahijani, P., Mohammadi, M., Zainal, Z. A., & Mohamed, A. R. (2015). Advances in CO2 gasification reactivity of biomass char through utilization of radio frequency irradiation. *Energy*, *93*, 976-983. https://doi.org/10.1016/j.energy.2015.09.092

11. Petrov, G. M., Apruzese, J. P., Petrova, T. B., & Wolford, M. F. (2016). Investigation of industrial-scale carbon dioxide reduction using pulsed electron beams. *Journal of Applied Physics*, *119*(10), 103303. https://doi.org/10.1063/1.4943620

12. Chmielewski, A. G. (2007). Industrial applications of electron beam flue gas treatment—From laboratory to the practice. *Radiation Physics and Chemistry*, *76*(8-9), 1480-1484. https://doi.org/10.1016/j.radphyschem.2007.02.056

13. Rebbert, R. E., Lias, S. G., & Ausloos, P. (1973). Pulse radiolysis of methane. *Journal of research of the National Bureau of Standards. Section A, Physics and chemistry*, *77*(2), 249. https://doi.org/10.6028/jres.077a.017

14. Hummel, R. W. (1963). The role of unsaturated products in the radiolysis of methane. *Discussions of the Faraday Society*, *36*, 75-82. https://doi.org/10.1039/DF9633600075

15. Arai, H., Nagai, S., & Hatada, M. (1982). Electron beam radiolysis of CH4/CO2 mixtures. *Zeitschrift für Physikalische Chemie*, *131*(1), 69-78. https://doi.org/10.1524/zpch.1982.131.1.069

16. Cahill, R. W., Seeler, A. K., & Glass, R. A. (1967). Formation of acetylene and other two-carbon compounds in methane with electron pulses. *The Journal of Physical Chemistry*, *71*(13), 4564-4566. https://doi.org/10.1021/j100872a072

17. Sieck, L. W., & Johnsen, R. H. (1963). SOME ASPECTS OF THE RADIATION CHEMISTRY OF METHANE 1. *The Journal of Physical Chemistry*, *67*(11), 2281-2288. https://doi.org/10.1021/j100805a009

18. Indarto, A., Choi, J. W., Lee, H., & Song, H. K. (2005). Kinetic modeling of plasma methane conversion using gliding arc. *J. Nat. Gas Chem*, *14*, 13-21.

19. Yang, Y. (2003). Direct non-oxidative methane conversion by non-thermal plasma: experimental study. *Plasma chemistry and plasma processing*, *23*(2), 283-296.https://doi.org/10.1023/A:1022924220062

20. Willis, C., & Boyd, A. W. (1976). Excitation in the radiation chemistry of inorganic gases. *International Journal for Radiation Physics and Chemistry*, *8*(1-2), 71-111. https://doi.org/10.1016/0020-7055(76)90061-9

21. Dong, X., Ninnemann, E., Ranasinghe, D. S., Laich, A., Greene, R., Vasu, S. S., & Green, W. H. (2020). Revealing the critical role of radical-involved pathways in high temperature cyclopentanone pyrolysis. *Combustion and Flame*, *216*, 280-292. https://doi.org/10.1016/j.combustflame.2020.03.001

22. Stagni, A., Song, Y., Vandewalle, L. A., Van Geem, K. M., Marin, G. B., Herbinet, O., ... & Faravelli, T. (2020). The role of chemistry in the oscillating combustion of hydrocarbons: An experimental and theoretical study. *Chemical Engineering Journal*, *385*, 123401. https://doi.org/10.1016/j.cej.2019.123401

23. Heijkers, S., Aghaei, M., & Bogaerts, A. (2020). Plasma-based CH4 conversion into higher hydrocarbons and H2: modeling to reveal the reaction mechanisms of different plasma sources. *The Journal of Physical Chemistry C*, *124*(13), 7016-7030. https://doi.org/10.1021/acs.jpcc.0c00082

24. Cui, Y., Zhang, H., Xu, H., & Li, W. (2007). Kinetic study of the catalytic reforming of CH4 with CO2 to syngas over ni/α-Al2O3 catalyst : The effect of temperature on the reforming mechanism. *Applied Catalysis. A, General*, 318, 79-88. https://doi.org/10.1016/j.apcata.2006.10.044

25. Ianni, James C. (2019) Kintecus Windows Version 6.80. www.kintecus.com.

26. Okazaki, K., Sato, S., & Ohno, S. I. (1976). The estimation of the G-values for ionization and excitation of ten-electron molecules: Methane, ammonia, and water irradiated by 100 keV electrons. *Bulletin of the Chemical Society of Japan*, *49*(1), 174-181. https://doi.org/10.1246/bcsj.49.174

27. Mätzing, H. (1991). Chemical kinetics of flue gas cleaning by irradiation with electrons. *Advances in chemical physics*, *80*, 315-402. https://doi.org/10.1002/9780470141298.ch4

28. Matveev, I. B., Ardelyan, N. V., Bychkov, V. L., Bychkov, D. V., & Kosmachevskii, K. V. (2013). Plasma assisted combustion, gasification and pollution control. *Int. Plasma Technol. Center*, *1*, 1-28. https://doi.org/10.1109/TPS.2007.911085

29. Anicich, V. G. (2003). An index of the literature for bimolecular gas phase cation-molecule reaction kinetics. *JPL-Publication-03-19* 1194

30. Schmitt, K. L., Murray, D. M., & Dibble, T. S. (2009). Towards a consistent chemical kinetic model of electron beam irradiation of humid air. *Plasma Chemistry and Plasma Processing*, 29(5), 347-362. https://doi.org/10.1007/s11090-009-9186-y

31. Didion, J. P., Martin, M., & Collins, F. S. (2017). Atropos: specific, sensitive, and speedy trimming of sequencing reads. *PeerJ*, 5, e3720. https://doi.org/10.7717/peerj.3720

32. Ianni, J. C. Atropos, V1.00 (2003). https://trs.jpl.nasa.gov/handle/2014/7981

33. Hiraoka, K., & Kebarle, P. (1975). Energetics, stabilities, and possible structures of CH5+ (CH4) n clusters from gas phase study of equilibriums CH5+ (CH4) n-1+ CH4= CH5+ (CH4) n for n= 1-5. *Journal of the American Chemical Society*, 97(15), 4179-4183. https://doi.org/10.1021/ja00848a005

34. Wang, B., Hou, H., Yoder, L. M., Muckerman, J. T., & Fockenberg, C. (2003). Experimental and theoretical investigations on the methyl− methyl recombination reaction. *The Journal of Physical Chemistry A*, *107*(51), 11414-11426. https://doi.org/10.1021/jp030657h

35. Sillesen, A., Ratajczak, E., & Pagsberg, P. (1993). Kinetics of the reactions H+ C2H4→ C2H5, H+ C2H5→ 2CH3 and CH3+ C2H5→ products studied by pulse radiolysis combined with infrared diode laser spectroscopy. *Chemical physics letters*, 201(1-4), 171-177. https://doi.org/10.1016/0009-2614(93)85052-P

36. Baulch, D. L., Bowman, C. T., Cobos, C. J., Cox, R. A., Just, T., Kerr, J. A., ... & Warnatz, J. (2005). Evaluated kinetic data for combustion modeling: supplement II. *Journal of physical and chemical reference data*, *34*(3), 757-1397. https://doi.org/10.1063/1.1748524

37. Gong, C., Yu, J., Wang, K., Liu, J., Huang, W., Si, X., ... & Han, Y. (2018). Numerical study of plasma produced ozone assisted combustion in a direct injection spark ignition methanol engine. *Energy*, 153, 1028-1037. https://doi.org/10.1016/j.energy.2018.04.096

38. Leng, X., Huang, H., Ge, Q., He, Z., Zhang, Y., Wang, Q., ... & Long, W. (2021). Effects of hydrogen enrichment on the combustion and emission characteristics of a turbulent jet ignited medium speed natural gas engine: A numerical study. *Fuel*, 290, 119966. https://doi.org/10.1016/j.fuel.2020.119966

39. Zhen, X., Wang, Y., & Liu, D. (2016). A new improvement on a chemical kinetic model of primary reference fuel for multi-dimensional CFD simulation. *Energy Conversion and Management*, 109, 113-121. https://doi.org/10.1016/j.enconman.2015.11.061

Table 1. Simulation conditions of four CH_4 electron beam radiolysis experiments.

	Temperature	Dose rate	Simulation time	G values reported
Arai et al. (1982)	393 K	50 kGy sec^{-1}	6 seconds	H_2, C_2H_6, C_2H_4, C_2H_2, C_3H_8
Hummel 1963	288 K	4.3 kGy sec^{-1}	*10 seconds	H_2, C_2H_6, C_4H_{10}
Cahill et al. (1967)	*298 K	112 kGy sec^{-1}	*10 seconds	H_2, C_2H_6
Sieck and Johnsen (1963)	*298 K	1 kGy sec^{-1}	*10 seconds	C_2H_6, C_3H_8, C_4H_{10}

* We use 298 K and 10 seconds for any temperature and simulation time not provided, respectively.

Table 2. Major sources of H_2 and their rate constants. "Number" refers to the order of appearance of the reaction in our mechanism, not the order of importance.

Rate constant (cm^3 $molecule^{-1}$ s^{-1})	Reaction	Number
9.0×10^{-14}	$C_2H_5^+ + CH_4 \rightarrow H_2 + C_3H_7^+$	(4)
1.1×10^{-9}	$CH_3^+ + CH_4 \rightarrow H_2 + C_2H_5^+$	(5)
2.7×10^{-10}	$H + CH_2 \rightarrow H_2 + CH$	(6)

Table 3. Major sources of C_2H_6 and their rate constants.

Rate constant (cm^3 $molecule^{-1}$ s^{-1})	Reaction	Number	% contribution at 0.5-second	% contribution at 6-second
5.5×10^{-11}	$CH_3 + CH_3 \rightarrow C_2H_6$	(9)	65	52
1.7×10^{-10}	$H + C_2H_5 \rightarrow C_2H_6$	(10)	16	13
4.8×10^{-10}	$C_2H_5^+ + C_3H_8 \rightarrow C_3H_7^+ + C_2H_6$	(11)	5	20
1.5×10^{-7}	$e^- + C_2H_7^+ \rightarrow H + C_2H_6$	(12)	12	14
4.9×10^{-10}	$C_2H_4^+ + C_3H_8 \rightarrow C_3H_6^+ + C_2H_6$	(13)	1	1

Table 4. Comparison of relative importance of reaction pathways of H_2 and C_2H_6 between our model (50 kGy sec^{-1}, 0.5 seconds) and Heijkers et al.[23] The "N/A" indicates the reaction is not contained in the model. Note that e^- as reactants in this Table correspond to thermal electons for our model (except where noted), whereas Heijkers et al. explicitly treat the full range of electron energy loss in interactions with CH_4 and other species.

	Rate constant (cm^3 $molecule^{-1}$ s^{-1})	Reaction	DBD	Our model
H_2	$f(\sigma)$ [a]	$e^- + CH_4 \rightarrow e^- + CH_2 + H_2$	34%	20% [b]
	9.0×10^{-14}	$C_2H_5^+ + CH_4 \rightarrow C_3H_7^+ + H_2$	N/A	19%
	1.1×10^{-9}	$CH_3^+ + CH_4 \rightarrow C_2H_5^+ + H_2$	0.3%	18%
	2.7×10^{-10}	$CH_2 + H \rightarrow CH + H_2$	20%	11%
	$f(\sigma)$	$e^- + CH_4 \rightarrow e^- + CH + H_2 + H$	0.3%	7% [a]
	1.5×10^{-7}	$e^- + C_2H_7^+ \rightarrow C_2H_5 + H_2$	N/A	6%
	1.0×10^{-9}	$C_2H_6 + CH_5^+ \rightarrow C_2H_5^+ + H_2 + CH_4$	3%	2%
	1.5×10^{-7}	$e^- + C_2H_5^+ \rightarrow H + C_2H_2 + H_2$	3%	<0.1%
	$f(\sigma)$	$e^- + C_2H_6 \rightarrow e^- + C_2H_4 + H_2$	34%	N/A
	$f(\sigma)$	$e^- + C_2H_4 \rightarrow e^- + C_2H_2 + H_2$	6.7%	N/A
	$f(\sigma)$	$e^- + C_3H_8 \rightarrow e^- + C_3H_6 + H_2$	0.3%	N/A
	6.9×10^{-15}	$CH_2 + H_2 \rightarrow CH_3 + H$	<0.1%	76%
	6.3×10^{-21}	$H_2 + C_3H_7 \rightarrow C_3H_8 + H$	>90%	<0.1%
C_2H_6	[c] 2.2×10^{-26}	$CH_3 + CH_3 + M \rightarrow C_2H_6 + M$	91%	65%
	2.3×10^{-10}	$C_2H_5 + H \rightarrow C_2H_6$	9%	16%
	$f(\sigma)$	$e^- + C_2H_6 \rightarrow e^- + C_2H_4 + H_2$	>90%	N/A
	1.0×10^{-9}	$C_2H_6 + CH_5^+ \rightarrow C_2H_5^+ + H_2 + CH_4$	0%	81%

a) Rate coefficients of electron impact reactions calculated using cross sections data[23]

b) Reaction 1

c) Rate constant unit : cm^6 $molecule^{-2}$ s^{-1}

Table 5. Percent difference in concentration of stable products between the original model and reduced mechanisms at 50 kGy sec^{-1} for 6-seconds.

Model size	H_2	C_2H_6	C_2H_4	C_2H_2	C_3H_8	C_4H_{10}
186	1.0%	-23.9%	-97.2%	-98.5%	159%	29.1%
247	-1.7%	2.9%	-12.2%	-36.6%	3.3%	2.5%
300	-0.6%	3.0%	-7.1%	-18.6%	1.3%	0.3%
331	-0.3%	0.7%	-3.8%	-4.8%	-0.5%	-0.1%
359	-0.4%	0.7%	-3.7%	-4.7%	-0.2%	0.3%

FIGURE 1 Concentrations vs. time for a set of major products during a 0.5 seconds simulation under a dose rate of 50 kGy sec–1. Note that [H2] and [C2H6] have been divided by ten

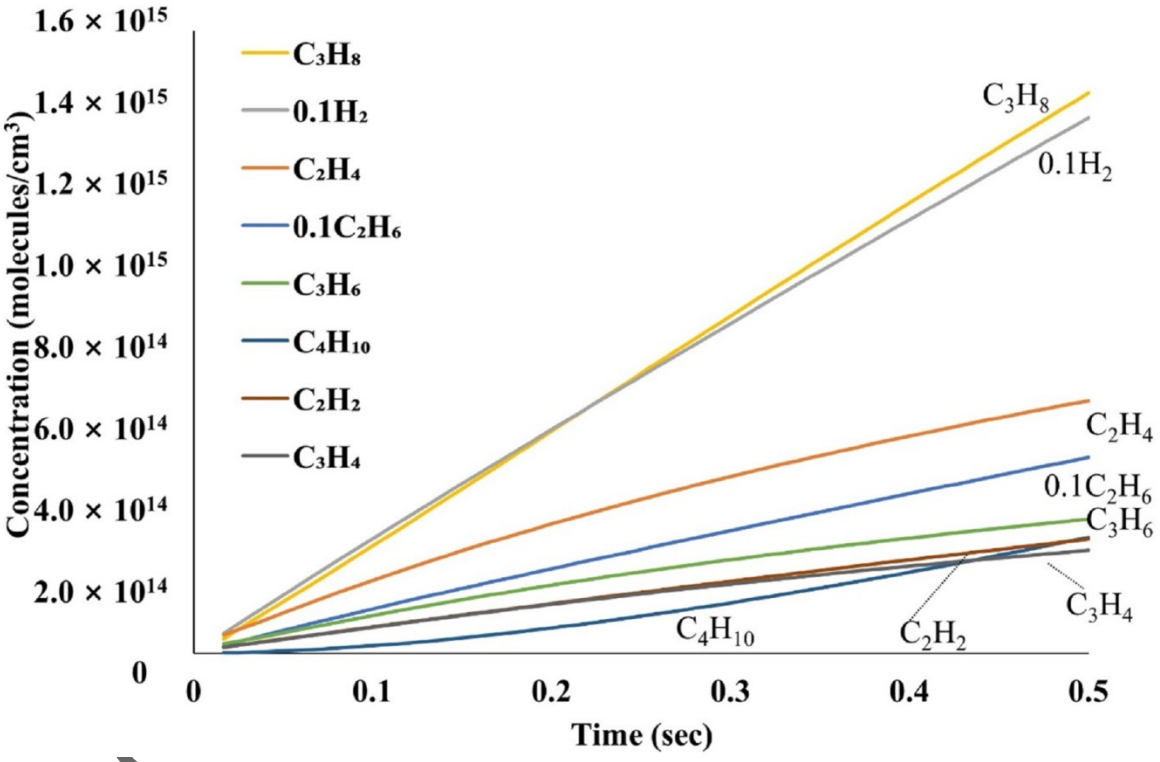

FIGURE 2 Concentrations vs. time for the major radicals during a 0.5-second simulation at a dose rate of 50 kGy sec–1. Note that [CH3] and [H] have been divided by ten

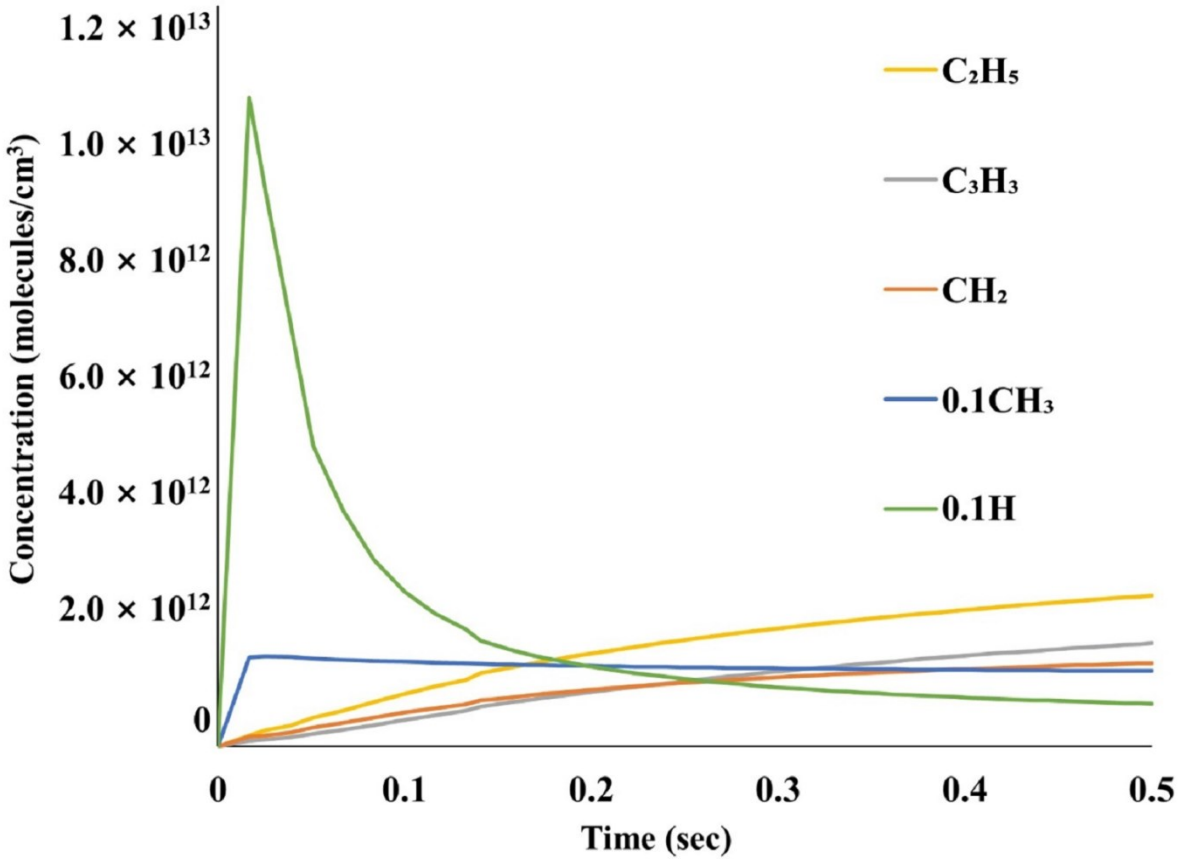

FIGURE 3 Concentrations vs. time for the of major ions during a 0.5 seconds simulation at a dose rate of 50 kGy sec–1. Note that [et–] has been divided by ten

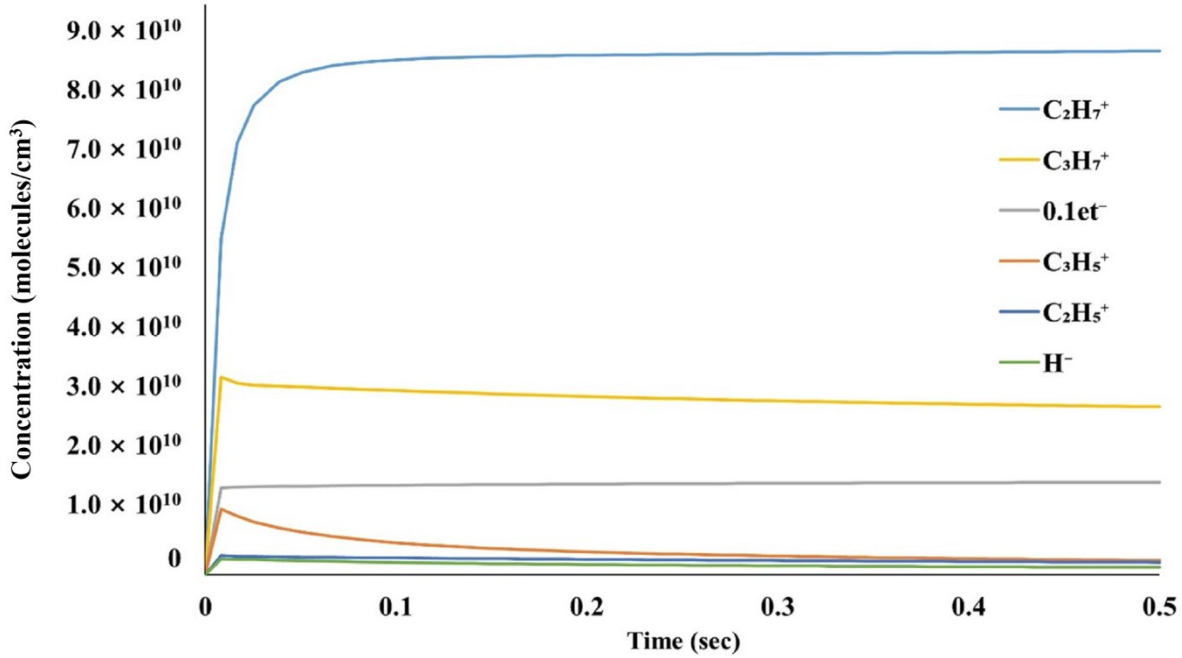

FIGURE 4 Comparison of simulated to experimental G-values for product formation in continuous irradiation experiments in pure CH4. For each experimental paper, we carried out a simulation (black symbols) specific to the dose rate and irradiation time of that paper, so for each product we present experimental results paired with the corresponding simulation result. Different experiments are coded by different shapes. Gvalues for C3H6 and C3H4 are not available in the literature

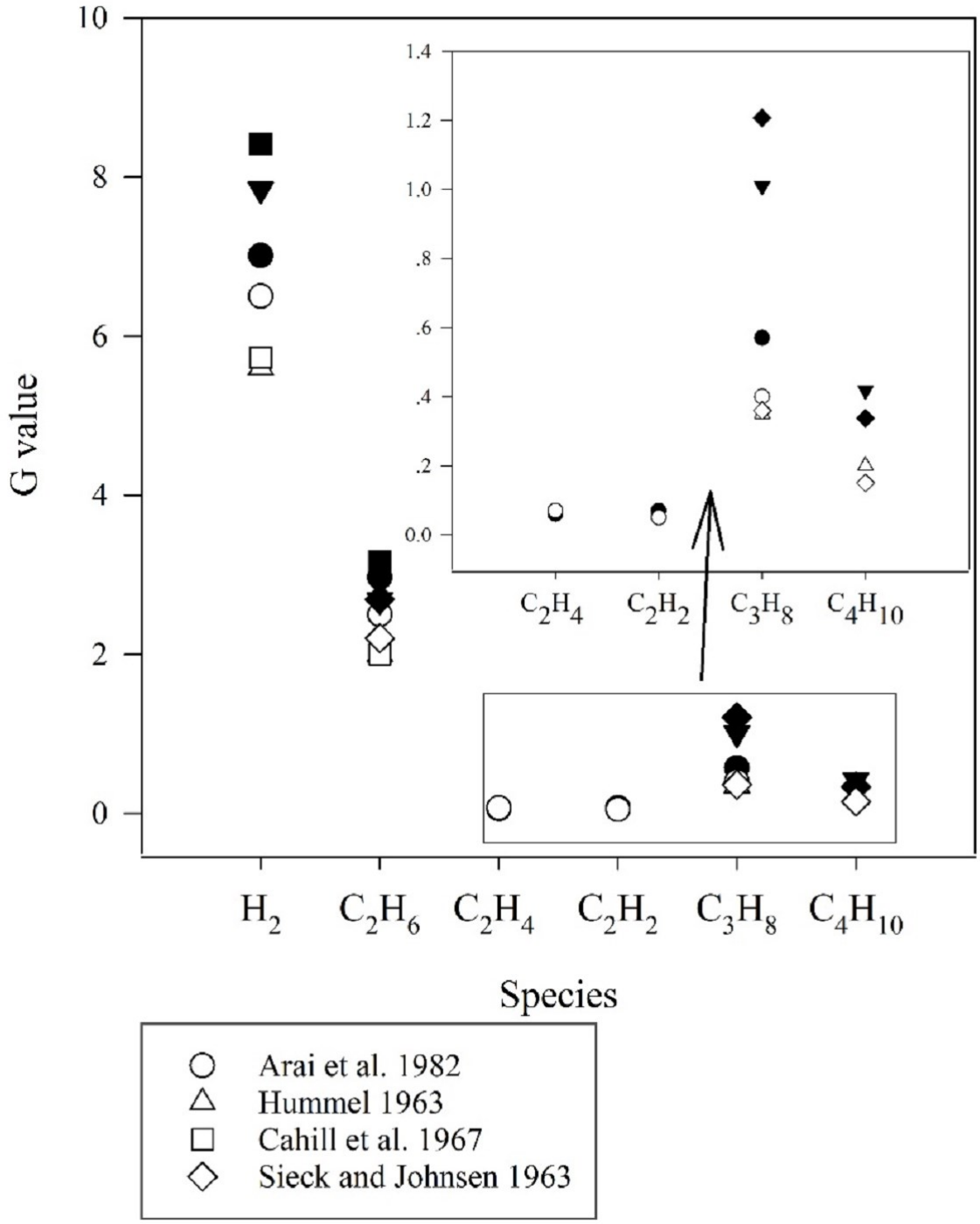

FIGURE 5 Relative importance of reactions contributing over 2% to the total production of H2 during a 0.5- second simulation at a dose rate of 50 kGy sec–1